

Semiclassical approach for excitonic spectrum of Coulomb coupling between two Dirac particles

Victor Zalipaev and Vladislav Kuidin
ITMO University, St. Petersburg, 197101, Russia*

The properties of energy spectrum of excitons in monolayer transition metal dichalcogenides are investigated using a multiband model. In the multiband model we use the excitonic Hamiltonian in the product base of the Dirac single-particle states at the conduction and valence band edges. Following the separation of variables we decouple the corresponding energy eigenvalue system of the first order ODE radial equations rigorously and solve the resulting the second order ODE self-consistently, using the finite difference method, thus we determine the energy eigenvalues of the discrete excitonic spectrum and the corresponding wave functions. We also developed WKB approach to solve the same spectral problem in semiclassical approximation for the resulting ODE. We compare the results for the energy spectrum and the corresponding eigen-functions forms for WS2 and WSe2 obtained by means of both methods. We also compare our results for the energy spectrum with other theoretical works for excitons, and with available experimental data.

I. INTRODUCTION

Two-dimensional atomically thin graphene-type materials such as TMD monolayers (MoS_2 , $MoSe_2$, WS_2 , WSe_2) with the stoichiometric formula MX_2 , where M represents a transition metal, like Mo or W, and X stands for a chalcogenide (S , Se , or Te) attract a high interest due to the fact that they display new fundamental physical properties that are expected to be important for future applications in electronics and optics with the emphasis in optoelectronics and photodetection, where optical absorption plays a central role [1–9]. It is therefore of utmost importance to understand the dominating optical absorption mechanism in 2D TMDs, which has strong excitonic character. In contrast to graphene, which has a gapless spectrum, the inversion symmetry breaking in TMD monolayers leads to the formation of a direct band gap. It is worth to mention that in [10] a rigorous approach of separation of variables was developed for the pure Coulomb potential that is opposite to the finite element analysis presented in [11] which was applied to the case the screened Coulomb potential - the Keldysh potential [12–14].

Moreover, it was understood that for ultra thin semiconductors the dielectric environment plays a crucial role and influences the effective strength of the Coulomb potentials inside a semiconductor layer (see [11]). Such long-range interactions become stronger as the thickness of the semiconductor layer decreases, which allows the formation of neutral and charged excitons. This enhanced Coulomb interaction leads to high exciton binding energies of neutral [1, 5, 15–18] and charged excitons [19–28] recently attracting a particular interest in the scientific community [29–31].

In our paper the properties of energy spectrum of excitons in TMD monolayer are investigated using a multiband model. The starting point of our analysis is the

excitonic Hamiltonian constructed in [11]. In this multiband model we use the excitonic Hamiltonian in the product base of the Dirac single-particle states at the conduction and valence band edges described in the paper [11]. This includes the effect of spin-orbit coupling, in the product base of the single-particle states at the conduction and valence band edges. Following the separation of variables we decouple the corresponding energy eigenvalue system of the first order ODE radial equations rigorously and solve the resulting the second order ODE self-consistently using the finite difference method. Thus we determine the energy eigenvalues of the discrete excitonic spectrum and the corresponding wave functions. We also developed WKB approach to solve the same spectral problem in the semiclassical approximation for the resulting ODE in the case of the Keldysh potential application. Similar to [10], [11], we compare the results for the energy spectrum and the corresponding eigen-functions forms for WS2 and WSe2 obtained by means of both methods. We also compare our results for the energy spectrum with the data presented in [10] for the excitonic s-states.

According to [11], the exciton Hamiltonian is constructed in the basis $(|\phi_c^e\rangle \otimes |\phi_v^h\rangle, |\phi_c^e\rangle \otimes |\phi_v^h\rangle, |\phi_c^e\rangle \otimes |\phi_v^e\rangle, |\phi_c^h\rangle \otimes |\phi_v^e\rangle, |\phi_c^e\rangle \otimes |\phi_v^h\rangle,)^T$, that is the basis states spanning the total Hilbert space that is given by the set of all the possible combinations of tensor products of the atomic orbital states of the individual particles at the conduction and valence band edges. Using the orthonormality of the basis functions, the total exciton Hamiltonian (symbol of the operator) could be written in the form introduced in [11] (see formulas (4) and (5)) with the Keldysh potential $-V(r)$ in polar coordinates that is given by [12–14]

$$V(r) = V_0 \frac{\pi}{2} \left(H_0 \left(\frac{r}{r_0} \right) - Y_0 \left(\frac{r}{r_0} \right) \right), \quad (1)$$

where $Y_0(r)$ and $H_0(r)$ are the Neumann function and the Struve function, respectively, r_0 is the screening

* vvezalipaev@itmo.ru

length (the characteristic space scale of the problem),

$$V_0 = \frac{e^2}{4\pi\epsilon_0\chi r_0 t}, \quad \chi = \frac{\epsilon_1 + \epsilon_2}{2}, \quad (2)$$

where t is the hopping parameter, $\epsilon_{1,2}$ is the dielectric constant of the environment above and below the TMD monolayer. It is worth remarking that $at = v_F \hbar$ where v_F is the Fermi velocity and a is the lattice constant.

The eigenvalue problem for this Hamiltonian

$$H_{\alpha}^{exc}(\mathbf{k}^e, \mathbf{k}^h, r_{eh})|\Psi_{\alpha,n}\rangle = E_{\alpha,n}^{exc}(\mathbf{k}^e, \mathbf{k}^h)|\Psi_{\alpha,n}\rangle \quad (3)$$

defines the exciton energy $E_{\alpha,n}^{exc}(\mathbf{k}^e, \mathbf{k}^h, r_{eh})$ and the exciton eigenstate $|\Psi_{\alpha,n}\rangle$, where α is a notation for the set of the spin and the valley indexes s_e, τ_e, s_h, τ_h with the values ± 1 for the electron-hole Dirac particles, $\mathbf{k}^e, \mathbf{k}^h$ are their wave numbers, n means a set of quantum numbers of the excitonic states of discrete spectrum ([11]). The above eigenvalue problem is a matrix equation which, following a procedure analogous to earlier works [32], [10] and [11], can be decoupled to a single ODE of the second kind.

II. SEPARATION OF VARIABLES FOR THE EXCITONIC HAMILTONIAN

Let us consider the excitons with zero center-of-mass momentum $\mathbf{K} = \mathbf{k}_e + \mathbf{k}_h = 0$. Introducing $\mathbf{k} \equiv \mathbf{k}_e = -\mathbf{k}_h$, and using transformation to dimensionless polar coordinates

$$\partial_x = \cos \varphi \partial_r - \frac{\sin \varphi}{r} \partial_{\varphi}, \quad \partial_y = \sin \varphi \partial_r + \frac{\cos \varphi}{r} \partial_{\varphi},$$

the exciton Hamiltonian (see Ref. [11]) can be written in the following way:

$$\begin{pmatrix} -V(r) & -he^{i\tau_h\varphi}D_h^- & -he^{-i\tau_e\varphi}D_e^+ & 0 \\ -he^{-i\tau_h\varphi}D_h^+ & \Delta_h - V(r) & 0 & -he^{-i\tau_e\varphi}D_e^+ \\ -he^{i\tau_e\varphi}D_e^- & 0 & -\Delta_e - V(r) & -he^{i\tau_h\varphi}D_h^- \\ 0 & -he^{i\tau_e\varphi}D_e^- & -he^{-i\tau_h\varphi}D_h^+ & \Lambda - V(r) \end{pmatrix}. \quad (4)$$

We define here differential operators $D_{e,h}^{\pm} \equiv i\tau_{e,h}\partial_r \pm \partial_{\varphi}/r$ and quantities $\Delta_{e,h} \equiv \Delta - \lambda s_{e,h}\tau_{e,h}$ (the effective band-gap, see [11]) with λ being the spin-orbit coupling strength, $\Lambda \equiv \lambda(s_e\tau_e - s_h\tau_h)$, and $h = a/r_0 = v_F\hbar/(r_0t)$ is the dimensionless parameter which is presumed to be small to apply WKB analysis. We have also expressed energy quantities ($\Delta, \lambda, V(r)$ etc.) in the hopping parameter t units and the spatial variables in the screening length r_0 ones.

Due to spin splitting of the valence band, there are effectively two band gaps and, as a consequence, two different types of excitons. These are commonly referred to as A and B excitons. The method presented in this paper can be applied with both values of $s_h\tau_h = \pm 1$.

When $s_h\tau_h = 1$ the hamiltonian (4) describes the A exciton, while $s_h\tau_h = -1$ relates to the B exciton. The A excitons in the K and K' valley have $s_e = 1, \tau_e = 1, s_h = -1, \tau_h = -1$ and $s_e = -1, \tau_e = -1, s_h = 1, \tau_h = 1$, respectively. The B exciton has $s_e = -1, \tau_e = 1, s_h = 1, \tau_h = -1$. Note that the intervalley exciton, which can arise due to excitation of charge carriers with linearly polarized light, also has $s_e\tau_e = s_h\tau_h$. Under such conditions we obtain $\Lambda = 0$.

For the A exciton in the K and K' valley (see [11]) we get

$$\Delta_h = \Delta_e = \Delta - \lambda = \Delta_{s,\tau}.$$

For the B exciton in the K valley (see [11]) we get

$$\Delta_h = \Delta_e = \Delta + \lambda.$$

Therefore, we can express Δ_h and Δ_e in terms of $\Delta_{s,\tau}$. In order to separate variables for the A and B excitons in the K valley, we use the ansatz

$$\psi(r, \varphi) = e^{il\varphi} \left(\psi_l^{(1)}(r)e^{-i\varphi}, \psi_l^{(2)}(r), \psi_l^{(3)}(r), \psi_l^{(4)}(r)e^{i\varphi} \right)^T,$$

where $l \in \mathbf{Z}$ is an orbital quantum number. Thus, the Hamiltonian (4) acting on

$$\psi_l(r) = \left(\psi_l^{(1)}(r), \psi_l^{(2)}(r), \psi_l^{(3)}(r), \psi_l^{(4)}(r) \right)^T$$

takes the form

$$\hat{H}_l = \begin{pmatrix} -V(r) & -hD_{-l} & hD_{-l} & 0 \\ -hD_l^\dagger & \Delta_{s,\tau} - V(r) & 0 & hD_{-l}^\dagger \\ hD_l^\dagger & 0 & -\Delta_{s,\tau} - V(r) & -hD_{-l}^\dagger \\ 0 & hD_l & -hD_l & -V(r) \end{pmatrix}, \quad (5)$$

where $D_l = -i\partial_r + \frac{il}{r}$, $D_l^\dagger = (-i\partial_r)^\dagger + \frac{il}{r}$, $(-i\partial_r)^\dagger = -i\partial_r - i/r$, or, equivalently, $\partial_r^\dagger = -\partial_r - 1/r$. Note that the Hamiltonian (5) is self-adjoint with respect to the scalar product

$$\langle \psi, \chi \rangle = \sum_{i=1}^4 \int_0^\infty \psi_i^*(r) \chi_i(r) r dr.$$

The spectral problem

$$\hat{H}_l \psi_{nl}(r) = E_{nl} \psi_{nl}(r), \quad n = 0, 1, 2, \dots, \quad (6)$$

for the Hamiltonian (5) with the radial quantum number n can be represented as the following system of four first-

order ODE's

$$\begin{cases} V_E \psi_l^{(1)} + ih \left(\partial_r + \frac{l}{r} \right) \psi_l^{(2)} - ih \left(\partial_r + \frac{l}{r} \right) \psi_l^{(3)} = 0, \\ \left(\partial_r - \frac{l-1}{r} \right) \psi_l^{(1)} - ih^{-1} (\Delta_{s,\tau} + V_E) \psi_l^{(2)} - \\ \left(\partial_r + \frac{l}{r} \right) \psi_l^{(4)} = 0, \\ \left(\partial_r - \frac{l-1}{r} \right) \psi_l^{(1)} + ih^{-1} (-\Delta_{s,\tau} + V_E) \psi_l^{(3)} - \\ \left(\partial_r + \frac{l}{r} \right) \psi_l^{(4)} = 0, \\ -ih \left(\partial_r - \frac{l-1}{r} \right) \psi_l^{(2)} + ih \left(\partial_r - \frac{l-1}{r} \right) \psi_l^{(3)} + V_E \psi_l^{(4)} = 0, \end{cases} \quad (7)$$

where $V_E = -V(r) - E$. Transforming vector components $\psi_l(r)$ into $\varphi_l^{(1,4)} = \psi_l^{(1)} \pm \psi_l^{(4)}$, $\varphi_l^{(2,3)} = \psi_l^{(2)} \pm \psi_l^{(3)}$, we obtain a new system of ODE for the components of a new vector $\varphi_l(r) = (\varphi_l^{(1)}, \varphi_l^{(2)}, \varphi_l^{(3)}, \varphi_l^{(4)})^T$. This system is reduced into a scalar second-order ODE

$$\left(\varphi_l^{(3)} \right)'' + \left(\frac{1}{r} - \frac{V'}{V_E} \right) \left(\varphi_l^{(3)} \right)' + \left(\frac{V_E^2 - \Delta_{s,\tau}^2}{4h^2} - \frac{l^2}{r^2} \right) \varphi_l^{(3)} = 0. \quad (8)$$

To separate variables for the A excitons in the K' value we have to use the ansatz

$$\psi(r, \varphi) = e^{i\varphi} \left(\psi_l^{(1)}(r) e^{i\varphi}, \psi_l^{(2)}(r), \psi_l^{(3)}(r), \psi_l^{(4)}(r) e^{-i\varphi} \right)^T.$$

As a result we obtain the same ODE (8).

We are going to calculate discrete spectrum of equation (8), assuming E the spectral parameter. We also assume that $E > 0$ as in this case the quantity $E + V(r)$ does not vanish. Otherwise, we have to deal with singularities. This case requires further studies. The coefficients of (8) depend on the spectral parameter E nonlinearly. Eigenfunctions $\varphi_l^{(3)}(r, E_n)$ are supposed to be square-integrable ($\varphi_l^{(3)}(r, E_n) \in L_2(0, +\infty)$). Taking into account that

$$V(r) = \frac{V_0}{r} + O(r^{-2})$$

as $r \rightarrow +\infty$, the coefficients in (8) could be simplified up to the leading order terms. This approximation results in the well-known Bessel-type ODE

$$\left(\varphi_l^{(3)} \right)'' + \frac{1}{r} \left(\varphi_l^{(3)} \right)' + \left(\frac{E^2 - \Delta_{s,\tau}^2}{4h^2} - \frac{l^2}{r^2} \right) \varphi_l^{(3)} = 0.$$

As we seek a solution decaying as $r \rightarrow +\infty$, the following inequality must hold

$$0 < E < \Delta_{s,\tau}. \quad (9)$$

As a result, we get the solution

$$\varphi_l^{(3)} \sim K_l(k_E r), \quad k_E = \frac{\sqrt{\Delta_{s,\tau}^2 - E^2}}{2h}, \quad (10)$$

where $K_l(r)$ is the MacDonald function that behaves as $e^{-r} \sqrt{\frac{\pi}{2r}}$ when $r \rightarrow +\infty$. Thus, the energy levels must satisfy the inequality (9).

Using the gauge transformation

$$\varphi_l^{(3)} = w(r) \exp \left(-\frac{1}{2} \int \left(\frac{1}{r} - \frac{V'}{V_E} \right) dr \right) = w(r) \sqrt{\frac{V_E}{r}}, \quad (11)$$

we change the equation (8) into the following self-adjoint, canonical form

$$w'' + Q(r, E)w = 0, \quad (12)$$

where

$$Q(r, E) = \frac{V_E^2 - \Delta_{s,\tau}^2}{4h^2} - \frac{l^2}{r^2} - \frac{1}{4} \left(\frac{1}{r} + \frac{V'}{V_E} \right)^2 - \frac{1}{2} \left(-\frac{1}{r^2} + \frac{V''}{V_E} + \left(\frac{V'}{V_E} \right)^2 \right).$$

It is clear that, when $r \rightarrow +\infty$, we have $Q \sim -k_E^2$, and one of the two linearly independent solutions of (12) decays exponentially.

Let us analyze the asymptotic behaviour of w as $r \rightarrow 0$. For the case $l \neq 0$, up to the leading order, we may use the approximation

$$Q(r, E) \sim \frac{1}{4r^2} - \frac{l^2}{r^2}. \quad (13)$$

As a result we obtain

$$w = C_1 r^{1/2+l} + C_2 r^{1/2-l}, \quad C_{1,2} = const. \quad (14)$$

Assuming $\varphi_l^{(3)}(r)$ bounded as $r \rightarrow 0$, we get $C_2 = 0$. Thus, for $l \neq 0$, we obtain that $w(0) = 0$.

For the case $l = 0$, up to the leading order, the following approximation may be used

$$Q(r, E) \sim \frac{1}{4r^2} - \frac{3}{4r^2 \log r^2}. \quad (15)$$

Then the solution would behave as

$$w \sim C \frac{r^{1/2}}{\sqrt{|\log r|}}, \quad C = const. \quad (16)$$

Thus, for $l = 0$, we obtain again that $w(0) = 0$.

As soon as compute $w(r)$ numerically, we can evaluate $\varphi_l^{(3)}(r)$ and the other components of $\varphi^l(r)$ and then all components of $\psi^l(r)$. Namely, we have

$$\varphi_l^{(1)} = \frac{2ilh}{r(E+V)} \varphi_l^{(3)}, \quad \varphi_l^{(4)} = \frac{2ih}{r(E+V)} \left(\varphi_l^{(3)} \right)', \quad (17)$$

$$\varphi_l^{(2)} = \frac{\Delta_{s,\tau}}{E+V} \varphi_l^{(3)}, \quad (18)$$

and

$$\psi_l^{(2,3)} = \frac{1}{2}\varphi_l^{(3)} \left(\frac{\Delta_{s,\tau}}{E+V} \pm 1 \right). \quad (19)$$

It is worth remarking that, if $l = 0$, we have

$$\psi_l^{(1)} = -\psi_l^{(4)} = \varphi_l^{(4)} = \frac{2i\hbar}{r(E+V)} \left(\varphi_l^{(3)} \right)', \quad (20)$$

and if $l \neq 0$, then

$$\psi_l^{(1)} = \frac{i\hbar}{V_E} \left(\frac{l}{r}\varphi_l^{(3)} + \left(\varphi_l^{(3)} \right)' \right), \quad (21)$$

$$\psi_l^{(4)} = \frac{i\hbar}{V_E} \left(\frac{l}{r}\varphi_l^{(3)} - \left(\varphi_l^{(3)} \right)' \right). \quad (22)$$

III. SEMICLASSICAL APPROACH FOR A AND B EXCITONS

In this section we solve the spectral problem for ODE (8) or (12) for $r \in [0, +\infty]$ analytically using semiclassical approximation (1D WKB approach) based on the method of comparison equation that is well-known in the theory of asymptotic methods in ODE (see for example [33], [34], [35]). It is worth remarking that semiclassical analysis has been successfully applied to many theoretical problems in graphene. We could mention briefly a few references: semiclassical approach to Berry phase analysis [36], the localized states [37] and Dirac electron tunnelling in graphene [38], [39]. When applying a semiclassical analysis, it is assumed that \hbar is a small parameter ($\hbar \ll 1$). For convenience, we also introduce a large parameter $k = 1/\hbar \gg 1$. Let us consider first the case with $l \neq 0$. Let us rewrite (12) in following way

$$w'' + k^2 q(r, E)w = 0, \quad (23)$$

where

$$q(r, E) = \frac{V_E^2 - \Delta_{s,\tau}^2}{4} - \hbar^2 q_h(r, E),$$

$$q_h = \frac{l^2}{r^2} + \frac{1}{4} \left(\frac{1}{r} + \frac{V'}{V_E} \right)^2 + \frac{1}{2} \left(-\frac{1}{r^2} + \frac{V''}{V_E} + \left(\frac{V'}{V_E} \right)^2 \right).$$

For this ODE we have got two turning points $r_{1,2} \in [0, +\infty]$, $r_1 < r_2$, for which $q(r_{1,2}, E) = 0$ that could locate close to each other. Thus, it is necessary to employ uniform asymptotic approximation relevant to the case when two turning points could coalesce (see [33], [34]). The approximation involves the parabolic special function $D_\nu(x)$ (see [35], [40]) that satisfies the following ODE

$$y'' + \left(\nu + \frac{1}{2} - \frac{x^2}{4} \right) y = 0, \quad (24)$$

and its asymptotic expansion for large x is given by

$$D_\nu(x) \sim e^{-x^2/4} x^\nu, \quad x \rightarrow +\infty.$$

Hence, the semiclassical approximation to the solution reads

$$w_n(r) = \left(\frac{d - z^2}{q(r, E_n)} \right)^{\frac{1}{4}} D_{kd/2-1/2}(\sqrt{2k}z), \quad (25)$$

$$d = \frac{2}{\pi} \int_{r_1}^{r_2} \sqrt{q(r, E_n)} dr.$$

The parameter z is to be found from the following equations: for $r > r_2$ ($q(r, E_n) < 0$, $z > \sqrt{d}$)

$$\int_{r_2}^r \sqrt{-q(r, E_n)} dr =$$

$$\frac{1}{2} \left(z\sqrt{z^2 - d} - d \log(z + \sqrt{z^2 - d}) \right) + \frac{d}{4} \log d. \quad (26)$$

For $r_1 < r < r_2$ ($q(r, E_n) > 0$, $-\sqrt{d} < z < \sqrt{d}$), we have

$$\int_{r_1}^r \sqrt{q(r, E_n)} dr =$$

$$\frac{1}{2} \left(z\sqrt{d - z^2} + d \arcsin \frac{z}{\sqrt{d}} \right) + \frac{\pi d}{4}. \quad (27)$$

Finally, for $r < r_1$ ($q(r, E_n) < 0$, $z < -\sqrt{d}$), z is to be found from

$$\int_r^{r_1} \sqrt{-q(r, E_n)} dr =$$

$$\frac{1}{2} \left(-z\sqrt{z^2 - d} - d \log(-z + \sqrt{z^2 - d}) \right) + \frac{d}{4} \log d. \quad (28)$$

The discrete spectrum $\{E_n\}_{n=0}^N$ is obtained from Bohr-Sommerfeld quantization rule (see [33], [34])

$$\int_{r_1}^{r_2} \sqrt{q(r, E_n)} dr = \pi \hbar \left(n + \frac{1}{2} \right). \quad (29)$$

However, the discussed above form of WKB approximation is not applicable to describe the case $l = 0$. In this situation for (23), we have got only one turning point r_1 , and the integral in the corresponding Bohr-Sommerfeld quantization rule diverges due to the singularity of $q(r, E) \sim 1/(4r^2)$ as $r \rightarrow 0$.

Thus, for the case $l = 0$, WKB analysis is to be developed in a different way. For ODE (8) the change of variable $r = e^t$ ($t \in (-\infty, +\infty)$) results in

$$(\varphi_l^{(3)})'' - \frac{d}{dt} \log(-V_E)(\varphi_l^{(3)})' + e^{2t} \frac{(E+V)^2 - \Delta_{s,\tau}^2}{4h^2} \varphi_l^{(3)} = 0. \quad (30)$$

Introducing a new dependent variable

$$u(t) = \frac{\varphi_l^{(3)}(r)}{\sqrt{E+V(r)}}, \quad (31)$$

we obtain

$$u'' + k^2 p(t, E)u = 0, \quad k \gg 1, \quad (32)$$

where

$$p(t, E) = e^{2t} \frac{(E+V)^2 - \Delta_{s,\tau}^2}{4} - h^2 \left(\frac{V''}{2V_E} + \frac{3V'^2}{4V_E^2} \right). \quad (33)$$

In this expression all derivatives are assumed to be evaluated with respect to the variable t .

For this ODE (32), we have got two turning points $t_{1,2} \in [-\infty, +\infty]$, $t_1 < t_2$, for which $p(t_{1,2}, E) = 0$ that are distinct from each other. Thus, it is reasonable to employ uniform asymptotic approximation for the case when two turning points do not coalesce (see [33], [34]), with the Airy special function $v(x) = \sqrt{\pi} Ai(x)$ that satisfies the following ODE $y'' - xy = 0$ ([35], [40]). Hence, we obtain for $t < t^*$

$$u_n(t) = C_0 k^{1/6} \left(\frac{z_1(t)}{p(t, E_n)} \right)^{1/4} v(-k^{2/3} z_1(t)), \quad (34)$$

and for $t > t^*$

$$u_n(t) = C_0 (-1)^n k^{1/6} \left(\frac{z_2(t)}{p(t, E_n)} \right)^{1/4} v(-k^{2/3} z_2(t)), \quad (35)$$

where t^* is an arbitrary point between t_1 and t_2 , and $C_0 = const$. For these asymptotic formulae, the real valued functions $z_{1,2}(t)$ are defined by

$$z_1(t) = - \left(\frac{3}{2} \int_t^{t_1} \sqrt{-p(t, E_n)} dt \right)^{2/3} < 0, \quad t < t_1, \quad (36)$$

$$z_1(t) = \left(\frac{3}{2} \int_{t_1}^t \sqrt{p(t, E_n)} dt \right)^{2/3} > 0, \quad t_1 < t < t^*, \quad (37)$$

$$z_2(t) = \left(\frac{3}{2} \int_t^{t_2} \sqrt{p(t, E_n)} dt \right)^{2/3} > 0, \quad t^* < t < t_2, \quad (38)$$

$$z_2(t) = - \left(\frac{3}{2} \int_{t_2}^t \sqrt{-p(t, E_n)} dt \right)^{2/3} < 0, \quad t > t_2. \quad (39)$$

It is worth noting that $p(t, E_n) < 0$ for $t < t_1$, $p(t, E_n) > 0$ for $t_1 < t < t_2$, and $p(t, E_n) < 0$ for $t > t_2$.

The discrete spectrum $\{E_n\}_{n=0}^N$ in this case is again obtained from the Bohr-Sommerfeld quantization rule

$$\int_{t_1}^{t_2} \sqrt{p(t, E_n)} dt = \pi h \left(n + \frac{1}{2} \right). \quad (40)$$

This quantization rule makes both asymptotic formulae (34) and (35) consistent.

IV. A EXCITON IN K VALLEY - NUMERICAL ANALYSIS

We confine our numerical analysis by considering the special case $s_e = \tau_e = 1$, $s_h = \tau_h = -1$ which corresponds to A exciton in K valley (see [11]) and was studied theoretically in the previous sections. On the basis of ODE (12), by truncating the semi-axes to the segment $[0, R]$, we solve our spectral problem using finite differences method (FDM) with following boundary conditions

$$w(0) = w(R) = 0. \quad (41)$$

We take into account that the eigenfunction must decay exponentially. Thus, the discrete version of (12) is the homogeneous system of linear algebraic equations that involves the energy spectral parameter in a nonlinear way

$$A(E)\bar{w} = 0. \quad (42)$$

The system is formed by the tridiagonal matrix $m \times m$ which entries are given by

$$A_{i,i}(E) = 4 - 2Q_i h_r^2, \quad A_{i,i+1}(E) = -h_r - 2,$$

$$A_{i+1,i}(E) = h_r - 2,$$

where $r_i = ih_r$, $i = 1, 2, \dots, m$, $h_r = R/(m+1)$, $Q_i = Q(r_i)$, $\bar{w} = (w_1, w_2, \dots, w_m)^T$, $w_i = w(r_i)$. The discrete excitonic spectrum is determined approximately by the equation $\det(A(E)) = 0$, which could be solved by iterative Newton method.

The described above numerical method is relatively simple and straightforward. Various tests demonstrated its stability with the increase of the size of the system m and the parameter R .

Fig. 1 shows comparison between the data for the excitonic spectrum E_{n0} for the s-states ($l = 0$) with $n = 0, 1, 2, 3$ obtained in [10], and the values computed on the basis of WKB approximation and FDM data. It has been done first for the example of WS2 with the parameters $\Delta_{s,\tau} = 2.4eV$, $a = 3.197A^0$, $t = 1.25eV$,

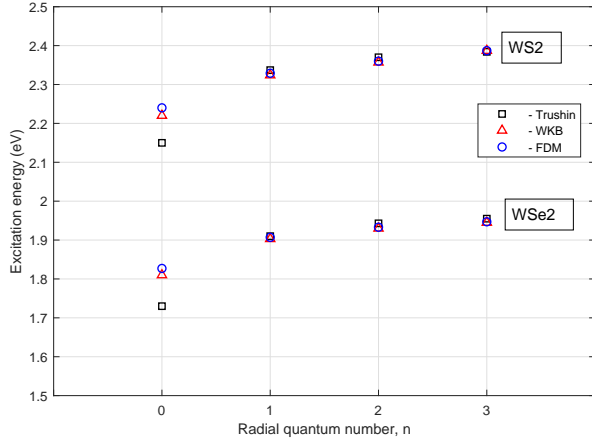


FIG. 1. The excitonic spectrum E_{n0} for the s-states ($l = 0$) with $n = 0, 1, 2, 3$ for two examples of WS2 and WSe2. The data of Trushin analytical solution (black squares) are shown for comparison together with the WKB approximation values (red triangles) and the finite difference method data (FDM, blue circles).

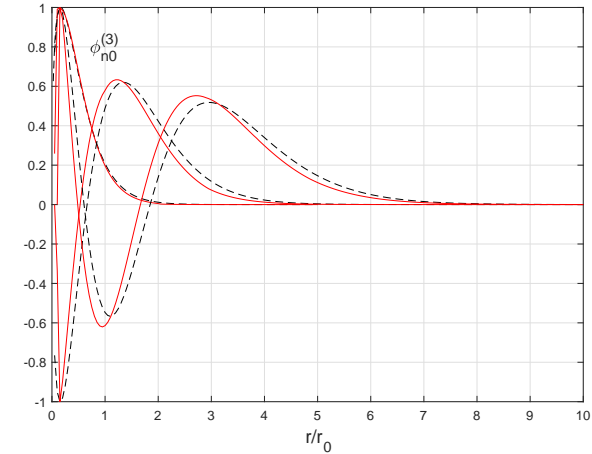


FIG. 2. FDM data (black dashed curves) versus WKB approximation values (red continuous curves) for the case $n = 0, 1, 2$ and $l = 0$ for WS2 example showing $\varphi_{n0}^{(3)}$ dependence on r .

and then, for the example of WSe2 with $\Delta_{s,\tau} = 1.97eV$, $a = 3.317A^0$, and $t = 1.13eV$. Both examples involve the SiO2 substrate with permittivity $\epsilon = 3.9$. For both examples we have $\hbar = 0.1157$. It is clear that the ground state energy obtained with FDM and WKB differs from analytical solution. The discrepancy of excited states, however, is relatively low. We have to take into account that semiclassical approximation works perfectly for relatively large quantization indices. It is worth remarking that analytical solution, as it was demonstrated in [10] agrees with the experimental data obtained in [41] and [42].

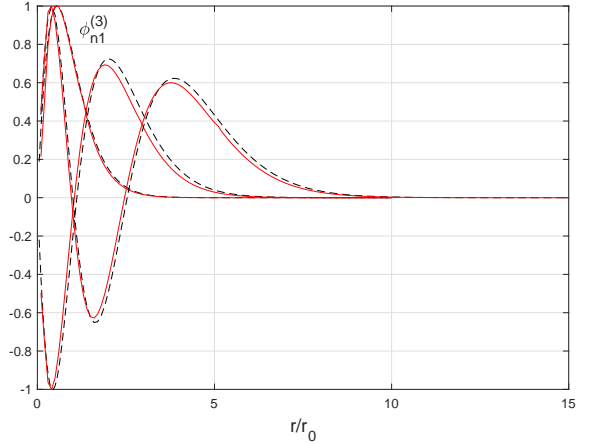


FIG. 3. FDM data (black dashed curves) versus WKB approximation values (red continuous curves) for the case $n = 0, 1, 2$ and $l = 1$ for WS2 example showing $\varphi_{n1}^{(3)}$ dependence on r .

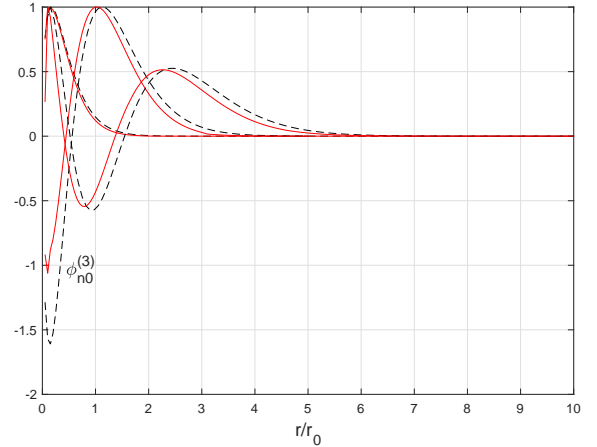


FIG. 4. FDM data (black dashed curves) versus WKB approximation values (red continuous curves) for the case $n = 0, 1, 2$ and $l = 0$ for WSe2 example showing $\varphi_{n0}^{(3)}$ dependence on r .

Below we compare the data obtained by means of WKB approximation and FDM for two examples of WS2 and WSe2 with the parameters described above. Thus in Fig. 2 and Fig. 3 for $l = 0, 1$, correspondingly, the behaviour of $\varphi_{nl}^{(3)}(r)$ with $n = 0, 1, 2$ is shown. The WKB approximation values are represented with red continuous curves, whereas FDM data are shown with black dashed curves. The values of E_{n0} for the s-states are shown in Fig 1. For the p-states, using WKB approximation, we obtain $E_{01} = 2.304eV$, $E_{11} = 2.351eV$, $E_{21} = 2.371eV$. The corresponding values computed with the help of FDM are $E_{01} = 2.310eV$, $E_{11} = 2.353eV$, $E_{21} = 2.371eV$. It is worth remarking that, for the values of $n = 1, 2$, the curves intersect the r axis one and two

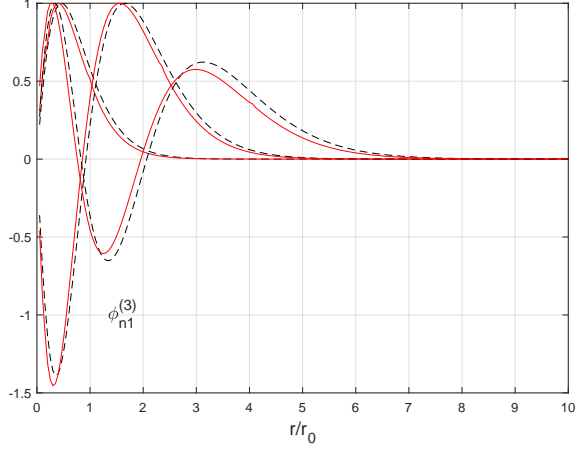


FIG. 5. FDM data (black dashed curves) versus WKB approximation values (red continuous curves) for the case $n = 0, 1, 2$ and $l = 1$ for WSe2 example showing $\varphi_{n1}^{(3)}$ dependence on r .

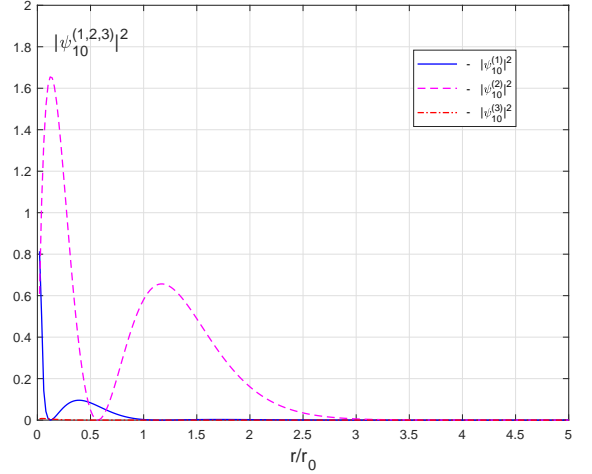


FIG. 7. Semiclassical approximation data for the probability distributions for the case $n = 1$ and $l = 0$ for WS2 example showing $|\psi_{10}^{(1,2,3)}|^2$ dependence on r .

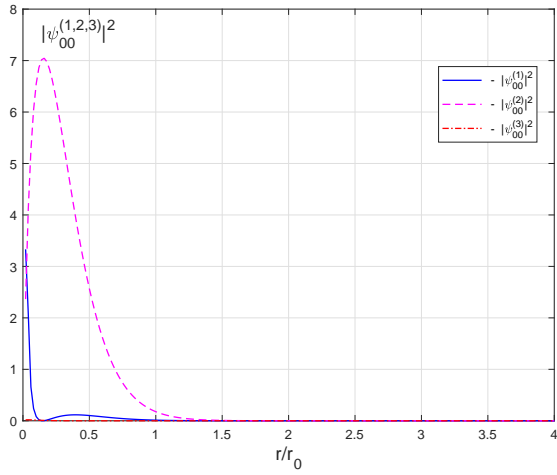


FIG. 6. Semiclassical approximation data for the probability distributions for the case $n = 0$ and $l = 0$ for WS2 example showing $|\psi_{00}^{(1,2,3)}|^2$ dependence on r .

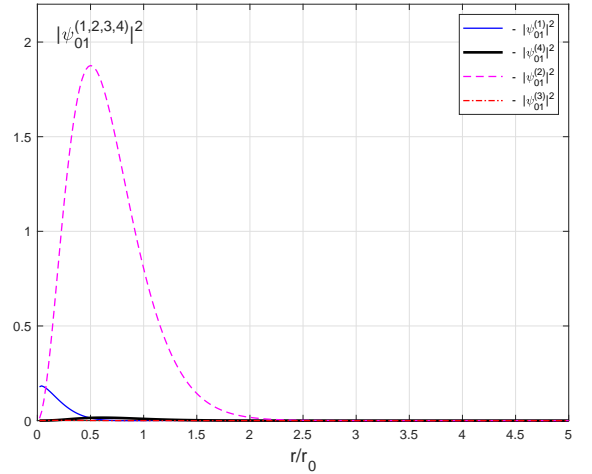


FIG. 8. Semiclassical approximation data for the probability distributions for the case $n = 0$ and $l = 1$ for WS2 example showing $|\psi_{01}^{(1,2,3,4)}|^2$ dependence on r .

times correspondingly, opposite to the case with $n = 0$ without intersection. In this case one could clearly observe the compliance of data.

Similarly, in Fig. 4 and Fig. 5, again for $l = 0, 1$ correspondingly, the behaviour of $\varphi_{nl}^{(3)}(r)$ with $n = 0, 1, 2$ also demonstrates good agreement between the WKB and FDM data. The values of E_{n0} for the s-states are shown in Fig 1. For the p-states, using WKB approximation, we obtained $E_{01} = 1.877eV$, $E_{11} = 1.921eV$, $E_{21} = 1.939eV$. The corresponding values computed with the help of FDM are $E_{01} = 1.882eV$, $E_{11} = 1.923eV$, $E_{21} = 1.940eV$. Thus, we have illustrated that both methods could provide reliable results.

In Fig. 6-9 for the WS2 example the dependence of

$|\psi_{n0}^{(1,2,3)}|^2$ and $|\psi_{n1}^{(1,2,3,4)}|^2$ on r for $n = 0, 1$ is demonstrated. All four figures show that the component $|\psi_{n0}^{(3)}|^2$ prevails with respect to the others.

V. CONCLUSION

The energy spectrum of excitons in monolayer transition metal dichalcogenides was calculated using a multi-band model. In this model, we used the excitonic Hamiltonian in the product base of single-particle states at the conduction and valence band edges constructed in [11]. Following the separation of variables, we decou-

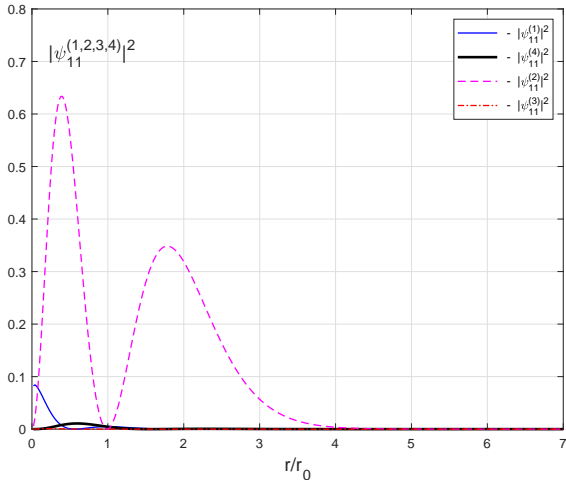


FIG. 9. Semiclassical approximation data for the probability distributions for the case $n = 1$ and $l = 1$ for WS2 example showing $|\psi_{11}^{(1,2,3,4)}|^2$ dependence on r .

pled the corresponding system of the first order ODE for the radial eigen-vector components and solved the resulting second order ODE using the finite difference method. Thus, we determined the energy levels of the electron-hole pairs and the corresponding eigen-states. We also developed WKB approach to solve this spectral problem in semiclassical approximation for the resulting ODE and demonstrated a very good agreement between the numerical data obtained by both methods. We also compared our results for the energy spectrum with other theoretical works for excitons.

ACKNOWLEDGMENTS

This work is supported by the Russian Science Foundation under Grant No. 18-12-00429. The authors would like to thank Dr Alexei Vagov, Dr Dmitry R. Gulevich and Yaroslav V. Zhumagulov for helpful discussions.

-
- [1] K. F. Mak, C. Lee, J. Hone, J. Shan, and T. F. Heinz, Atomically thin MoS₂: A new direct-gap semiconductor, *Phys. Rev. Lett.* **105**, 136805 (2010).
 - [2] A. Ramasubramaniam, Large excitonic effects in monolayers of molybdenum and tungsten dichalcogenides, *Phys. Rev. B* **86**, 115409 (2012).
 - [3] D. Xiao, G.-B. Liu, W. Feng, X. Xu, and W. Yao, Coupled spin and valley physics in monolayers of MoS₂ and other group-VI dichalcogenides, *Phys. Rev. Lett.* **108**, 196802 (2012).
 - [4] A. Kormányos, G. Burkard, M. Gmitra, J. Fabian, V. Zólyomi, N. D. Drummond, and V. Fal'ko, k-ptheory for two-dimensional transition metal dichalcogenide semiconductors, *2D Mater.* **2**, 022001 (2015).
 - [5] A. Splendiani, L. Sun, Y. Zhang, T. Li, J. Kim, C.-Y. Chim, G. Galli, and F. Wang, Emerging photoluminescence in monolayer MoS₂, *Nano Lett.* **10**, 1271 (2010).
 - [6] K. F. Mak, K. He, J. Shan, and T. F. Heinz, Control of valley polarization in monolayer MoS₂ by optical helicity, *Nat. Nanotechnol.* **7**, 494 (2012).
 - [7] H. Zeng, J. Dai, W. Yao, D. Xiao, and X. Cui, Valley polarization in MoS₂ monolayers by optical pumping, *Nat. Nanotechnol.* **7**, 490 (2012).
 - [8] T. Cao, G. Wang, W. Han, H. Ye, C. Zhu, J. Shi, Q. Niu, P. Tan, E. Wang, B. Liu, and J. Feng, Valley-selective circular dichroism of monolayer molybdenum disulphide, *Nat. Commun.* **3**, 887 (2012).
 - [9] G. Sallen, L. Bouet, X. Marie, G. Wang, C. R. Zhu, W. P. Han, Y. Lu, P. H. Tan, T. Amand, B. L. Liu, and B. Urbaszek, Robust optical emission polarization in MoS₂ monolayers through selective valley excitation, *Phys. Rev. B* **86**, 081301 (2012).
 - [10] M. Trushin, M. O. Goerbig, and W. Belzig, Optical absorption by dirac excitons in single-layer transition-metal dichalcogenides, *Physical Review B* **94**, 041301 (2016).
 - [11] M. Van der Donck, M. Zarenia, and F. Peeters, Excitons and trions in monolayer transition metal dichalcogenides: A comparative study between the multiband model and the quadratic single-band model, *Physical Review B* **96**, 035131 (2017).
 - [12] N. S. Rytova, The screened potential of a point charge in a thin film, *Moscow University Physics Bulletin* **3**, 18 (1967).
 - [13] L. V. Keldysh, Coulomb interaction in thin semiconductor and semimetal films, *Soviet Journal of Experimental and Theoretical Physics Letters* **29**, 658 (1979).
 - [14] P. Cudazzo, I. V. Tokatly, and A. Rubio, Dielectric screening in two-dimensional insulators: Implications for excitonic and impurity states in graphane, *Phys. Rev. B* **84**, 085406 (2011).
 - [15] H.-P. Komsa and A. V. Krashennnikov, Effects of confinement and environment on the electronic structure and exciton binding energy of MoS₂ from first principles, *Phys. Rev. B* **86**, 241201 (2012).
 - [16] J. Feng, X. Qian, C.-W. Huang, and J. Li, Strain-engineered artificial atom as a broad-spectrum solar energy funnel, *Nat. Photonics* **6**, 866 (2012).
 - [17] D. Y. Qiu, F. H. da Jornada, and S. G. Louie, Optical spectrum of MoS₂: Many-body effects and diversity of exciton states, *Phys. Rev. Lett.* **111**, 216805 (2013).
 - [18] I. B. Amara, E. B. Salem, and S. Jaziri, Optoelectronic response and excitonic properties of monolayer MoS₂, *J. Appl. Phys.* **120**, 051707 (2016).
 - [19] K. F. Mak, K. He, C. Lee, G. H. Lee, J. Hone, T. F. Heinz, and J. Shan, Tightly bound trions in monolayer MoS₂, *Nat. Mater.* **12**, 207 (2012).
 - [20] J. S. Ross, P. Klement, A. M. Jones, N. J. Ghimire, J. Yan, D. G. Mandrus, T. Taniguchi, K. Watanabe, K. Kitamura, W. Yao, D. H. Cobden, and X. Xu, Electrically tunable excitonic light-emitting diodes based on monolayer WSe₂ p-n junctions,

- Nat. Nanotechnol. **9**, 268 (2014).
- [21] C. Lui, A. Frenzel, D. Pilon, Y.-H. Lee, X. Ling, G. Akselrod, J. Kong, and N. Gedik, Trion-induced negative photoconductivity in monolayer MoS₂, Phys. Rev. Lett. **113**, 166801 (2014).
- [22] A. R. Rezk, B. Carey, A. F. Chrimes, D. W. M. Lau, B. C. Gibson, C. Zheng, M. S. Fuhrer, L. Y. Yeo, and K. Kalantar-zadeh, Acoustically-driven trion and exciton modulation in piezoelectric two-dimensional MoS₂, Nano Lett. **16**, 849 (2016).
- [23] C. Zhang, H. Wang, W. Chan, C. Manolatou, and F. Rana, Absorption of light by excitons and trions in monolayers of metal dichalcogenide MoS₂: Experiments and theory, Phys. Rev. B **89**, 205436 (2014).
- [24] S. Mouri, Y. Miyauchi, and K. Matsuda, Tunable photoluminescence of monolayer MoS₂ via chemical doping, Nano Lett. **13**, 5944 (2013).
- [25] A. Singh, G. Moody, K. Tran, M. E. Scott, V. Overbeck, G. Berghäuser, J. Schaibley, E. J. Seifert, D. Pleskot, N. M. Gabor, J. Yan, D. G. Mandrus, M. Richter, E. Malic, X. Xu, and X. Li, Trion formation dynamics in monolayer transition metal dichalcogenides, Phys. Rev. B **93**, 041401 (2016).
- [26] N. Scheuschner, O. Ochedowski, A.-M. Kaulitz, R. Gillen, M. Schleberger, and J. Maultzsch, Photoluminescence of freestanding single- and few-layer MoS₂, Phys. Rev. B **89**, 125406 (2014).
- [27] R. Soklaski, Y. Liang, and L. Yang, Temperature effect on optical spectra of monolayer molybdenum disulfide, Appl. Phys. Lett. **104**, 193110 (2014).
- [28] Y. Zhang, H. Li, H. Wang, R. Liu, S.-L. Zhang, and Z.-J. Qiu, On valence-band splitting in layered MoS₂, ACS Nano **9**, 8514 (2015).
- [29] Y. V. Zhumagulov, A. Vagov, N. Y. Senkevich, D. R. Gulevich, and V. Perebeinos, Three-particle states and brightening of intervalley excitons in a doped mos₂ monolayer, Phys. Rev. B **101**, 245433 (2020).
- [30] Y. V. Zhumagulov, A. Vagov, D. R. Gulevich, P. E. Faria Junior, and V. Perebeinos, Trion induced photoluminescence of a doped mos₂ monolayer, The Journal of Chemical Physics **153**, 044132 (2020), <https://doi.org/10.1063/5.0012971>.
- [31] A. Arora, N. K. Wessling, T. Deilmann, T. Reichenauer, P. Steeger, P. Kossacki, M. Potemski, S. M. de Vasconcelos, M. Rohlfing, and R. Bratschitsch, Dark trions govern the temperature-dependent optical absorption and emission of doped atomically thin semiconductors, arXiv preprint arXiv:1911.06252 (2019).
- [32] O. L. Berman and R. Y. Kezerashvili, High-temperature superfluidity of the two-component bose gas in a transition metal dichalcogenide bilayer, Physical Review B **93**, 245410 (2016).
- [33] F. Olver, *Asymptotics and special functions* (CRC Press, 1997).
- [34] M. V. Fedoryuk, *Asymptotic analysis: linear ordinary differential equations* (Springer Science & Business Media, 2012).
- [35] V. A. Borovikov, Uniform stationary phase method, IEE Electromagnetic waves series **40** (1994).
- [36] P. Carmier and D. Ullmo, Berry phase in graphene: Semiclassical perspective, Physical Review B **77**, 245413 (2008).
- [37] V. Zalipaev, High-energy localized eigenstates in a fabry-perot graphene resonator in a magnetic field, Journal of Physics A: Mathematical and Theoretical **45**, 215306 (2012).
- [38] V. Zalipaev and C. Linton, Semiclassical analysis of tunneling through a smooth potential barrier and localized states in graphene monolayer with mass gap, Nanosystems: Physics, Chemistry, Mathematics **4**(6), 725 (2013).
- [39] V. Zalipaev, C. Linton, M. Croitoru, and A. Vagov, Resonant tunneling and localized states in a graphene monolayer with a mass gap, Physical Review B **91**, 085405 (2015).
- [40] M. Abramowitz and I. Stegun, *Handbook on Mathematical Functions with Formulas, Graphs, and Mathematical Tables. Chapter 19 on parabolic cylinder functions.* (Dover, New York, 1965).
- [41] A. Chernikov, T. C. Berkelbach, H. M. Hill, A. Rigosi, Y. Li, O. B. Aslan, D. R. Reichman, M. S. Hybertsen, and T. F. Heinz, Exciton binding energy and nonhydrogenic rydberg series in monolayer ws₂, Physical review letters **113**, 076802 (2014).
- [42] K. He, N. Kumar, L. Zhao, Z. Wang, K. F. Mak, H. Zhao, and J. Shan, Tightly bound excitons in monolayer wse₂, Physical review letters **113**, 026803 (2014).